

ON THE ENERGY LOSS BY  
FISSION FRAGMENTS ALONG  
THEIR RANGE

BY

N. O. LASSEN



KØBENHAVN

I KOMMISSION HOS EJNAR MUNKSGAARD

1949

## Erratum.

Page 21, note 1: for  $P\sigma$   $\alpha$ -particles read  $P\alpha$   $\alpha$ -particles.

D. Kgl. Danske Vidensk. Selskab, Mat.-fys. Medd. XXV. 11, N. O. Lassen.

## CONTENTS

	Page
Introduction.....	1
Chapter I. Specific Ionization in Argon	
§ 1. Experimental arrangement.....	1
§ 2. Experimental method.....	1
§ 3. Investigation of the proportionality between ionization and pulse size.....	1
§ 4. Distribution of specific ionization for various distances traversed.....	11
§ 5. Distribution curves for small values of $x$ .....	14
§ 6. Ionization range curves.....	17
Chapter II. Specific Ionization in Various Gases	
§ 1. Specific ionization in xenon.....	20
§ 2. Specific ionization in the light gases.....	21
§ 3. Comparison of various gases.....	21
§ 4. Measurements in mixtures of gases.....	23
Chapter III. Construction of Velocity Range Relations for the whole Range	
§ 1. Energy loss along the range in argon.....	31
§ 2. Energy range curves and velocity range curves in argon.....	33
§ 3. Energy loss along the range in the light gases.....	35
§ 4. Energy range curves and velocity range curves in hydrogen and deuterium.....	36
§ 5. Estimate of the effective charge of the fragments.....	39
Note added in proof.....	42
References.....	43

## INTRODUCTION

From cloud-chamber studies by BØGGILD, BROSTRØM, and LAURITSEN (1) it is known that the curve giving the energy loss by fission fragments along their range differs from the corresponding curve for  $\alpha$ -particles. The ionization produced by the fragments is high at the beginning of the path; it decreases along the range, reaching a minimum near the end of the track. In the very end the energy loss per cm is expected to rise again.

According to theoretical considerations regarding the penetration of fission fragments through matter as developed by BOHR (2), the range of the fragments may be divided into two parts over which the stopping mechanisms are essentially different. In the first part, where the fragment velocity is high compared with the orbital velocities of the most loosely bound electrons in the atoms of the stopping material, the energy loss takes place primarily through excitation and ionization of the atoms. In such electronic collisions the fragment with its bound electrons, having a total charge  $z^*$ , is assumed to act as a single particle of charge number  $z^*$ . The total charge is determined by a balance between capture and loss of electrons from the fragment ion, equilibrium being established when the most loosely bound electron in the fragment ion has an orbital velocity comparable with the translatory velocity  $v$  of the fragment. Consequently, the charge decreases as the fragment is slowed down, a phenomenon which has also been verified experimentally (3). Due to this decrease of  $z^*$ , the ionization decreases along the range, in contrast to the case of  $\alpha$ -particles or protons which exhibit an increasing ionization with decreasing velocity.

When the fragment reaches a velocity of the order of  $v_0 = \frac{e^2}{\hbar}$  it becomes almost completely neutralized. Moreover, in collisions

with the atoms, the electron structures tend to react adiabatically and, hence, the rate of energy loss in electronic collisions becomes very small. Due to their large mass, the fragments still have a considerable energy of several  $MeV$  and may thus cover an appreciable distance before being finally stopped. Over this residual part of the range, the energy loss is supposed to take place mainly in nuclear collisions, i. e. in encounters where kinetic energy is imparted to the stopping atom as a whole. From the theory it follows that the energy loss per cm due to such nuclear encounters increases towards the end of the path.

In the cloud-chamber experiments the increase in the number of nuclear collisions along the range was directly observed, but the energy loss per cm was determined in a somewhat indirect way by means of statistical methods. More direct measurements of the specific ionization in the first part of the range were performed by the author. The results obtained for argon have already been briefly reported elsewhere (4). Chapter I of the present paper gives a more detailed account of these experiments, while Chapter II deals with corresponding investigations in other gases. Finally, in Chapter III, an attempt is made to construct the range-velocity curve for the whole range by combining the ionization measurements with the cloud chamber experiments.

## CHAPTER I

### Specific Ionization in Argon.

#### § 1. Experimental arrangement.

The experimental arrangement is shown in Fig. 1. Inside a box, made of a 5" copper tube with a bottom and a removable lid, is placed a shallow ionization chamber. The collecting electrode is a brass plate mounted on the lid of the box by means of three amber supports (not shown in the figure). The second electrode is a thin foil of aluminum or gold held by a framework of brass, which is also mounted on the lid by means of amber supports. The distance between the two electrodes is  $5.0 \pm 0.1$  mm, the electrodes being as nearly parallel as possible. Inside the box

is furthermore placed a uranium layer, evaporated upon a mica sheet which is fastened to a brass plate. In front of the layer a diaphragm with about 350 openings is mounted; this diaphragm only allows the fission fragments to come out nearly perpendicularly to the surface of the layer. The whole "gun" is mounted on a brass rod which slides in a brass tube, and can be operated from outside; the air-tightening is made by means of a piece of rubber tubing greased with ricinolein. The gun as viewed

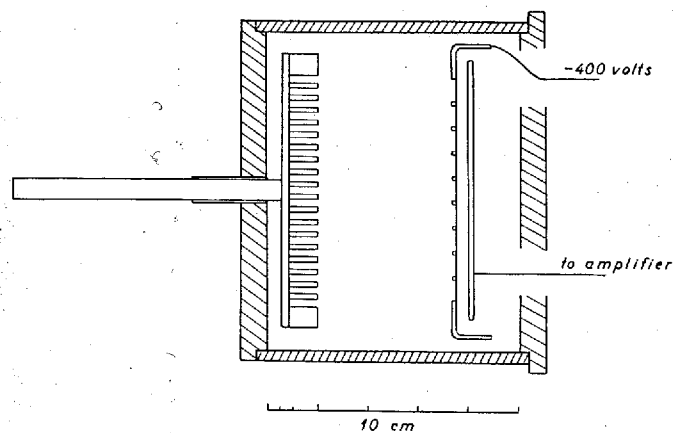
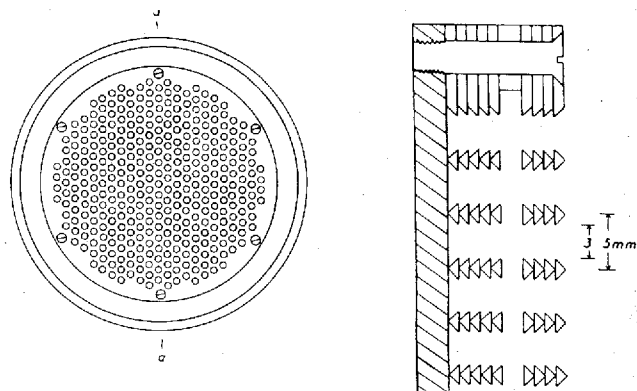


Fig. 1. Experimental arrangement.

from the right side in the picture is shown in Fig. 2a; Fig. 2b gives part of the cross-section  $a-a$  in enlarged scale. The diaphragm actually consists of nine brass plates, 1 mm thick, and a distance ring, 2 mm thick. The arrangement shown in the figure minimizes the number of fragments reflected from the walls of the channels to the ionization chamber. Later, however, this precaution was found to be unnecessary.

From the geometry described it is easily calculated that the distance traversed by the most obliquely moving fragments is 70 per cent higher than the distance traversed by the fragments moving perpendicularly to the surface. When the unavoidable small deviations from planeness of the foil and from parallelism of the electrodes are taken into account, the distances traversed by the various fragments inside the chamber are estimated to be equal within  $\pm 4$  per cent, while the distances traversed on the way to the chamber are equal within  $\pm 2.5$  per cent. Due to

the obliquely moving fragments the average distance traversed by the fragments before observation is 3 per cent higher than the distance between the uranium layer and the middle of the ionization chamber. The corresponding stopping equivalent  $x$  is obtained when the pressure of the argon inside the box, measured with a mercury manometer, is taken into account, and when the stopping equivalent of the aluminum foil is added.  $x$  can be varied by moving the gun and by varying the pressure. The



Figs. 2 a and 2 b.

mean thickness of the uranium layer is  $0.33 \text{ mg/cm}^2$  as determined by weighing as well as by  $\alpha$ -counting and it gives rise only to a small correction to  $x$  ( $\sim \frac{1}{2} \cdot 0.6 \text{ mm}$  of argon), which has been neglected. The layer is not exactly homogeneous, but the thickness is estimated to vary by less than 20 per cent.

The fission fragments are produced by slow neutrons hitting the uranium layer. The box is placed between the coils of the cyclotron at a distance of about 25 cm from an internal Be-target which is bombarded by deuterons and thus acts as a strong source of neutrons. 3—5 cm of paraffin are inserted between the target and the box which on all sides is surrounded by paraffin.

## § 2. Experimental method.

The ionization chamber is connected to a linear amplifier and a cathode-ray oscillograph whose screen is photographed on a continuously moving film. Fig. 3 shows a piece of a film. The

larger pulses are due to fission fragments, the actual pulses being directed upwards; the peaks going downwards are caused by the amplifier. Pulses due to statistical fluctuations of the background ionization caused by the intense irradiation with  $\gamma$ -rays and fast neutrons also occur. Numerous small pulses, partly separated from each other, are seen on the oscillograph, but on the rather slowly moving film they appear as a considerable broadening of the zero line. The recording films are placed in a small diaspocope and the measurements are always carried out in the same way. The number of pulses of various pulse sizes is counted and the distribution curve obtained is plotted.



Fig. 3.

Fig. 4 gives the result of two measurements in which the pressure in the box was 300 mm Hg of argon, the distance traversed by the fragments inside the ionization chamber thus corresponding to about 2 mm of argon at atmospheric pressure. The distance  $x$  from the uranium layer to the middle of the ionization chamber was equivalent to approximately 10 and 12 mm of argon at atmospheric pressure in the left and right curves, respectively. The curves give the number of pulses plotted against their sizes as measured in relative units (regarding the scale of abscissae, see later). The distribution of pulse sizes for  $x = 10 \text{ mm}$  shows the presence of the well-known two groups of fragments. Furthermore, it indicates that a few background pulses are much larger than is indicated by the breadth of the zero line and that some of the pulses due to the heavy group of fragments are smaller than the upper limit for the background pulses while, on the other hand, the light group is completely separated from the heavy group and the background.

From the curve can be determined the values of the abscissae corresponding to the two peaks, i. e. the most frequent sizes of the pulses of the two groups. It is possible approximately to

define what may be denoted as "the upper and lower limits" of the light group and "the upper limit" of the heavy group as the points of intersection between the steepest tangents to the curve and the axis of abscissae. Of course, the limits so obtained

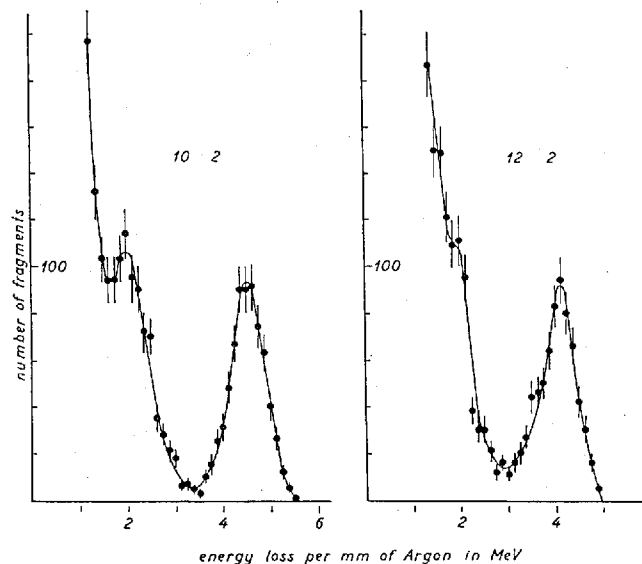


Fig. 4. Distribution of specific ionization by fission fragments having traversed 10 mm of argon (left) and 12 mm of argon (right). Depth of ion chamber corresponds to 2 mm of argon.

are only significant if the spread in pulse size caused by the background is considerably smaller than the width of each of the peaks. This is actually the case, as was shown by means of artificial pulses produced by an apparatus described earlier (5).

The artificial pulses were also used for testing the linearity of the amplifier; during each measurement they were frequently used for checking the amplification which did not remain strictly constant with time. In the various measurements during each series it was furthermore found convenient to use different amplifications of the last stage, and relative measures for the total amplification were obtained by means of the artificial pulses.

### § 3. Investigation of the proportionality between ionization and pulse size.

The magnitude of the background depends on the resolving time of the amplifier. In order to reduce the background to a reasonable amount it was necessary to choose the smallest time constant  $\tau$  of the amplifier rather low,  $\sim 3 \cdot 10^{-5}$  sec. However, while the negative ions were collected in a shorter time, it can easily be calculated from the known ionic mobility of the positive ions that complete collection of the latter required a somewhat longer time than  $\tau$ , although the field intensity used was rather high, 800 volts/cm. Accordingly, the pulse sizes were found to depend somewhat on the voltage across the chamber. This is an inconvenience, but it does not severely hamper the use of the apparatus. If the interdependence between pulse size and voltage is due solely to the rather small  $\tau$  in connection with the slow movements of the positive ions, the pulse sizes must be expected to be proportional to the number of ions as long as the voltage and the pressure are kept constant. In fact, for all fragments the conditions in the ionization chamber are nearly identical, the fragments all moving almost parallel to each other. Hence, the collection of the ions will take place quite similarly in the different cases. This means, firstly, that all the negative ions will be collected in a very short time; secondly, that within equal time intervals equal fractions of the total number of positive ions will be collected and, thirdly, that non-collected ions will be displaced by equal lengths. Thus, the shape of the voltage variation with time on the collector plate is the same for each pulse, and the pulse sizes give a relative measure for the ionization. We are, however, unable to perform a calibration by means of  $\alpha$ -particles in the usual way, since  $\alpha$ -particles moving in the same direction as do the fragments produce too low ionization inside the ionization chamber, and  $\alpha$ -particles moving parallel to the plates are unsuitable, since the collection of the ions formed by such particles will take place in a different way.

That the pulse sizes depend on the voltage might also partly be due to lack of saturation and, if this is the case, we shall obtain pulses roughly proportional to  $n(1 - \alpha n)$ , where  $n$  is the number of primary ion pairs and  $\alpha$  is the coefficient of re-

combination; hence, the larger pulses will be measured relatively too small. Now, since the fragments are moving perpendicularly to the plates, the negative ions have to move through a cloud of positive ions before reaching the collector plate, a fact which tends to increase a possible recombination. Therefore, it is necessary to investigate whether or not the pulse sizes are proportional to the number of primary ions.

The curves in Fig. 4 were obtained with 400 volts across the

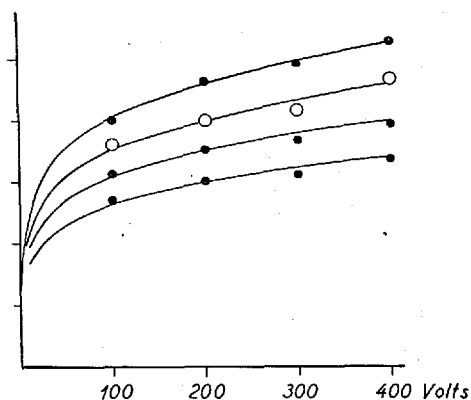


Fig. 5. Abscissa: voltage across the ion chamber. — Ordinates: pulse sizes in relative units. — Open circles correspond to the peak of the light group, full circles to upper and lower limits of the light group and upper limit of the heavy group.

chamber. For  $x = 10$  mm similar curves were determined with 300, 200, and 100 volts. In Fig. 5 the values of the pulse sizes are compared. As is seen, a doubling of the voltage corresponds to an increase in pulse size of about 15 per cent. The ordinates of the curves of Fig. 5 have a constant ratio, and the experimentally found points seem to agree fairly well with the assumption of proportionality.

In Table 1 the pulse sizes are given in relative units, the size of the upper limit of the light group being put equal to 1 for each voltage. If recombination takes place the small pulses will be measured relatively too high, an effect which will be the larger, the lower the voltage. Hence, it follows that the figures in the vertical columns should increase downwards, the increase being highest in the last column. In fact, the figures seem to point at a small variation just in this way. However, we conclude that the pos-

Table 1.

Volts	Light group			Heavy group
	Upper limit	Peak	Lower limit	Upper limit
400	1.00	0.88	0.74	0.63
300	1.00	.85	.74	.63
200	1.00	.87	.76	.65
100	1.00	.90	.79	.68

sible recombination can be neglected at 300 or 400 volts and that, for these voltages, the pulse sizes are proportional to the number of primary ions?

#### § 4. Distribution of specific ionization for various distances traversed.

From Fig. 4 it can be seen that the pulses are larger for  $x = 10$  mm than for  $x = 12$  mm. In the latter case, the pulses due to the light group are still clearly separated from the other pulses, while the heavy group has nearly disappeared in the background. For  $x = 14$  mm the pulses are further decreased (Fig. 6) and the heavy group cannot be seen any more; the pulses of the light group are also lowered and the separation between the latter and the other pulses is less complete. For  $x = 16, 18,$  and  $20$  mm (Fig. 7) the process continues and, in the last case, the light group has also disappeared into the background and can no longer be observed directly. Yet, the distribution curve obtained for  $x = 22$  mm (not shown) is slightly steeper than that for  $x = 20$  mm and, thus, the presence of fission fragments for  $x = 20$  mm can be detected.

The curves of Fig. 8 were obtained with a pressure of 150 mm Hg, the distance traversed by the fragments inside the chamber thus being equal to about 1 mm of argon at atmospheric pressure. The shape of the distribution curve for  $x = 10$  mm must, of course, be the same as that shown in Fig. 4 and, in fact, the agreement is satisfactory. The influence of the background seems to be slightly higher at lower pressure but, apart from this, the

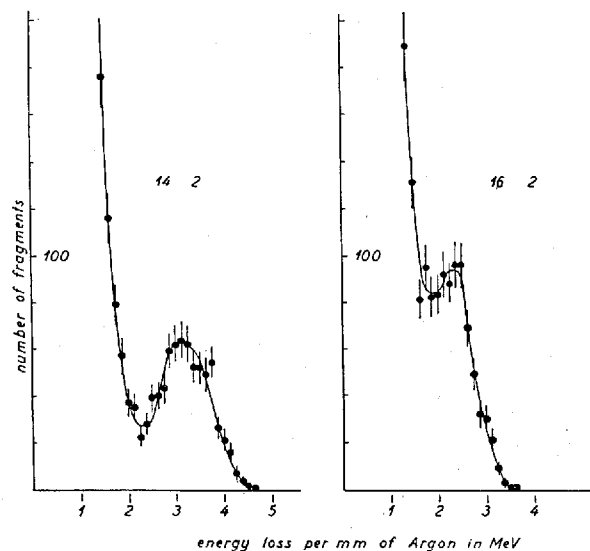


Fig. 6. Specific ionization for  $x = 14$  mm (left) and  $x = 16$  mm (right).  
 $\Delta x = 2$  mm.

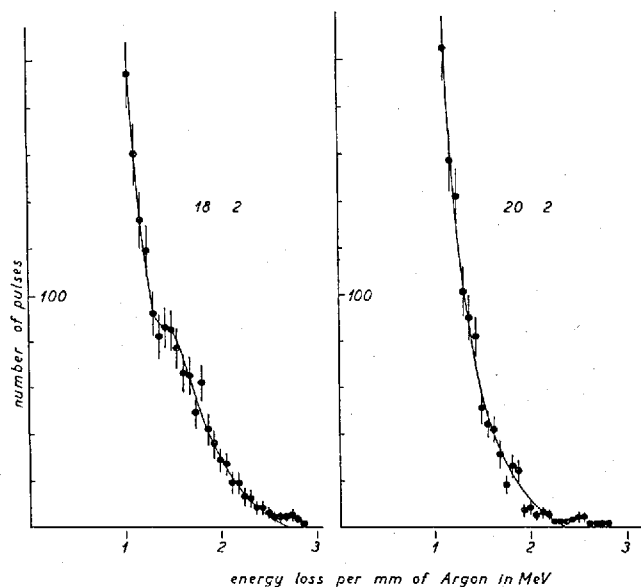


Fig. 7. Specific ionization for  $x = 18$  mm (left) and  $x = 20$  mm (right).  
 $\Delta x = 2$  mm.

two curves are very similar. The agreement between the absolute values of the abscissae is insignificant, because it is a result of the particular way of determining the scale (see later). Only for measurements performed at the same pressure the pulse sizes can be compared directly. The curves of Fig. 8 for  $x = 8$  and  $x = 10$  mm indicate that the pulse sizes increase for both groups of fragments when  $x$  is lowered. A closer examination of the figure shows that the increase is highest for the heavy group, an obser-

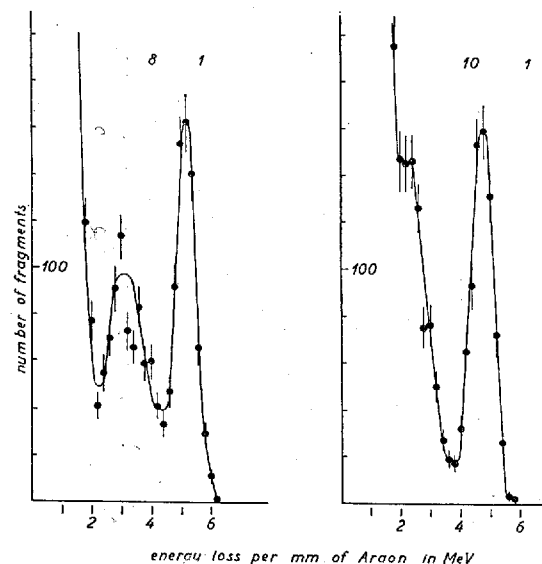


Fig. 8. Specific ionization for  $x = 8$  mm (left) and  $x = 10$  mm (right).  
 $\Delta x = 1$  mm.

vation which can also be deduced from the change in shape of the distribution curve. The two peaks of the curve have approached each other, which is clearly seen as the valley between the peaks is not so deep for  $x = 8$  mm as for  $x = 10$  mm.

When  $x$  is further decreased the pulse sizes increase further. Fig. 9 shows curves obtained at a pressure of 75 mm Hg. It is clearly seen that the two groups have come still closer to each other for  $x = 6$  mm and that they can no longer be separated for  $x = 4$  mm. Also the pulse sizes are higher for  $x = 4$  mm than for  $x = 6$  mm.

Although the peaks on the distribution curves are considerably

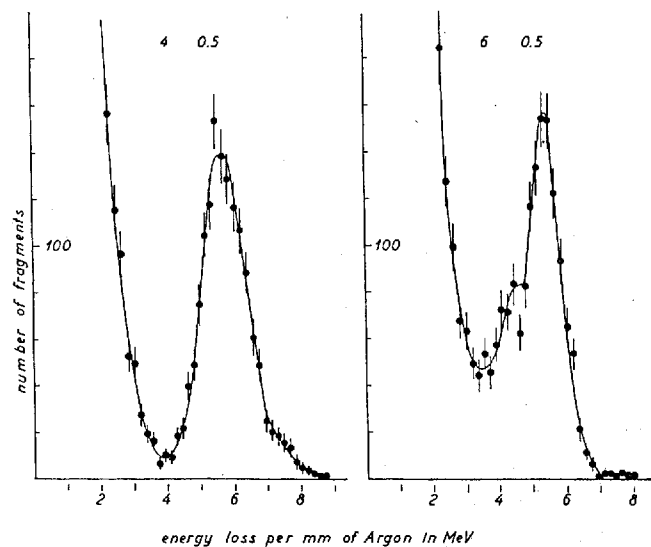


Fig. 9. Specific ionization for  $x = 4$  mm (left) and  $x = 6$  mm (right).  
 $\Delta x = 0.5$  mm.

broadened by the influence of the background and the finite geometry it appears that the two peaks are of different shapes, the heavy group being lower and broader than the light group. This was also to be expected since the spread of the total energy is higher for the heavy than for the light group.

### § 5. Distribution curves for small values of $x$ .

It is seen that the specific ionization decreases along the path of the fragment and that near the beginning of the path the decrease is higher for the heavy group. This indicates that the curves giving the specific ionization along the range for the two groups will intersect at an  $x$ -value of about 4 mm, and the single peak in Fig. 9 may be expected to split up into two peaks again when  $x$  is decreased below 4 mm. However, it was desirable to verify this expectation experimentally. This could not be done easily without changing the apparatus because of the rather large thickness of the gun and of the aluminum foil covering the ionization chamber.

An attempt was made to measure the ionization of the frag-

ments immediately outside the uranium layer. In a hemispherical ionization chamber, fission fragments were allowed to come out from a very thin uranium layer in directions diverging less than  $60^\circ$  from the normal. Their paths inside the chamber had the same lengths, corresponding to about 1 mm of argon at atmospheric pressure. The distribution curve for the ionization had only one peak, but this was unsymmetrical, having a hump on

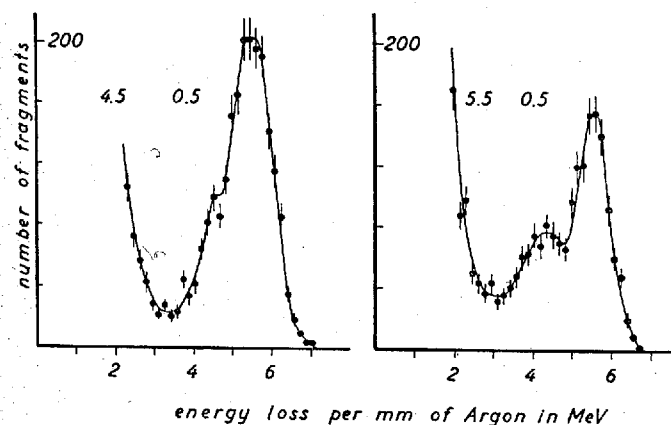


Fig. 10. Specific ionization for  $x = 4.5$  mm (left) and  $x = 5.5$  mm (right).  
 $\Delta x = 0.5$  mm.

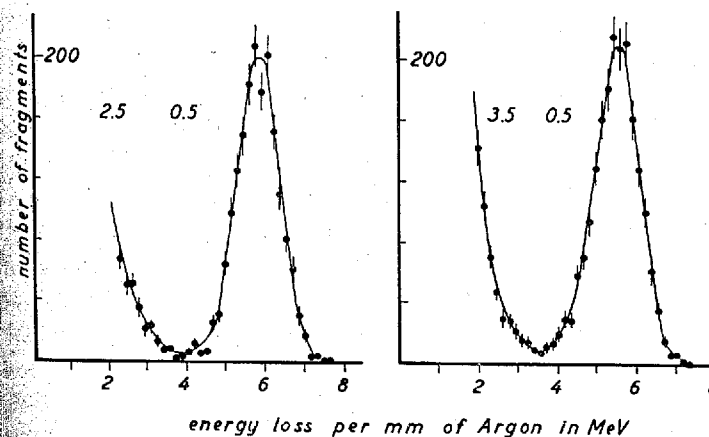


Fig. 11. Specific ionization for  $x = 2.5$  mm (left) and  $x = 3.5$  mm (right).  
 $\Delta x = 0.5$  mm.

the right side. However, since some amplification took place in the chamber, the measurements were not regarded as sufficiently reliable.

Therefore, after some minor alterations, further measurements were performed with the first arrangement. The gun was provided with a new diaphragm, a 3 mm thick circular aluminum plate with 3000 holes, 1 mm in diameter. The aluminum foil (0.25 mg/cm<sup>2</sup>  $\approx$  1.7 mm of argon) was replaced by a gold foil,

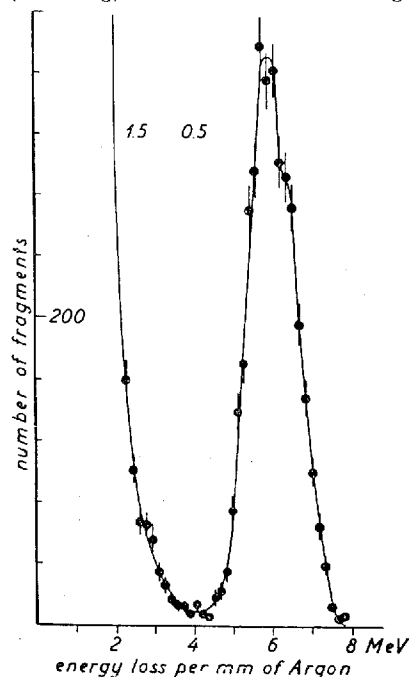


Fig. 12. Specific ionization for  $x = 1.5$  mm.  $\triangle x = 0.5$  mm.

and that the pulses due to the heavy group increase more rapidly when  $x$  varies from 5.5 to 3.5 mm. For  $x = 1.5$  the curve shows a peak with a hump on the right side and, though it cannot be decided with certainty which of the two groups has the higher ionization, it is most likely that the rate of increase of pulse sizes for the two groups has been continued also for values of  $x$  varying from 3.5 to 1.5 and, hence, that the heavy group corresponds to the higher pulse sizes. The hump of the curve is rather small, but additional indication for its existence was provided by the mentioned mea-

0.18 mg/cm<sup>2</sup>, corresponding to a stopping power of about 0.5 mm argon.

Figs. 10, 11, and 12 give the distribution curves for  $x$ -values, 1.5–5.5 mm, obtained with this arrangement and a pressure of 75 mm Hg. The agreement with previous measurements is satisfactory; the last figures, however, probably give the best curves, since here the background seems to be slightly smaller, which may be due to a small change in the position of the box or the thickness of the paraffin inserted between the Be-target and the box.

From the figures it is seen that the pulses due to the light group are slightly increased

measurements with the hemispherical chamber and also by a measurement with the present arrangement at a lower pressure. The latter measurement gave a very similar curve for  $x = 1.0$  mm (not shown).

## § 6. Ionization range curves.

In Fig. 13 the ionization values obtained are plotted against the distance  $x$  traversed by the fragments before the observation. The pulse sizes are measured in relative units, and for measurements performed at 300 mm Hg, corresponding to  $x$ -values of 10–20 mm, the values determined directly are plotted. The values obtained at 150 mm Hg, corresponding to  $x$ -values of

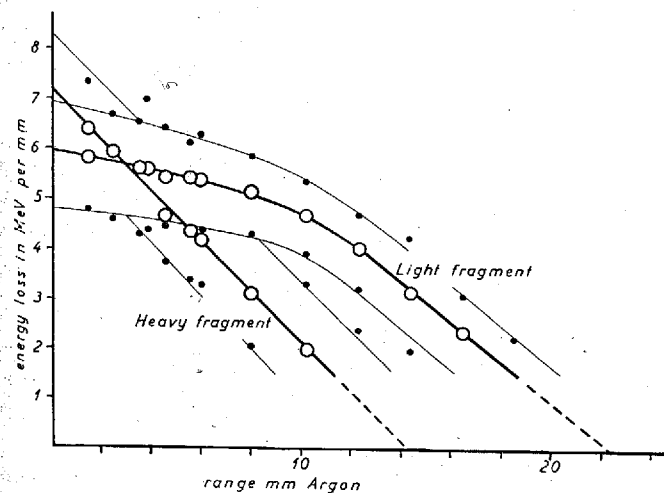


Fig. 13. Ionization range relations for fission fragments in argon. Open circles correspond to the peaks on the ionization distribution curves in the preceding figures, full circles to upper and lower limits. Regarding the scale of ordinates, see text.—When one of the peaks lies near the background the peak will be slightly displaced against the background. Similar phenomena occur when the two peaks lie near together. Small corrections are applied to compensate for this effect.

6–12 mm, are reduced by a suitable factor before plotting and in this way the range-ionization curves are fitted together. The transformation factor was determined by measurements of the ratio between the pulse sizes obtained at 300 mm Hg and at 150 mm Hg, respectively, for  $x$ -values of 10 and 12 mm. The

Table 2.  
Light group.

	Upper limit	Peak	Lower limit
$x = 10$ mm . . . .	0.77	0.76	0.77
$x = 12$ - . . . .	.81	.83	.81

ratio is given in Table 2, from which the mean value is found to be 0.79.

The measurements performed at a pressure of 75 mm Hg and by means of the first and the second diaphragm have been treated in a similar way. Two different transformation factors must be used, because different voltages (300 and 400 volts) were applied to the chamber in the respective experiments. Table 3 gives the factors used.

The scale of ordinates of Fig. 13 is chosen such that the area beneath the curve corresponding to the most frequent value of the specific ionization of the light group is 86 MeV. The value for the total energy given by FLAMMERSFELD, JENSEN, and GENTNER (6) is 87 MeV, but the absorption in the uranium layer may be slightly higher in the present experiments. The area beneath the corresponding curve for the heavy group is then found to be 52 MeV, the ratio of the areas thus being 1.65; this value agrees fairly well with the ratio 1.50 taken from the work of FLAMMERSFELD et al. Moreover, in the mentioned measurements we are dealing with that part of the range where the energy loss is almost entirely due to electronic collisions. By extrapolating the curves in the way shown they reach the axis of abscissae

Table 3.

Pressure	Diaphragm	Transformation factor	Range interval
300 mm Hg	No. 1	1.00	10—20 mm
150 - -	- 1	0.79	6—12 -
75 - -	- 1	0.70	4— 8 -
75 - -	- 2	0.63	1.5— 5.5 -

points corresponding to what may be called the extrapolated ranges  $R_{ex}$ . Since, as was mentioned in the Introduction, the fragments may traverse a considerable distance after the point where the ionization due to electronic collisions has decreased to zero, the actual ranges  $R$  may, however, be somewhat higher than  $R_{ex}$  and, hence, the areas beneath the curves drawn do not correspond exactly to the total energies.

These results do not agree with the conclusions of DEMERS (7) based on studies of the density of fission tracks in photographic plates, which point to a higher initial ionization of the light fragment than of the heavy fragment. Similar evidence was also recently obtained by SHERR and PETERSON (8) in an analysis of the shape of pulses from an ionization chamber.

The question therefore arises whether there is any possibility that, in the present experiments, the ionization  $E'_2$  by the heavy group should be measured systematically too high as compared with the corresponding quantity  $E'_1$  for the light group. In this connection it might be mentioned that small deviations from proportionality between pulse sizes and number of ions might arise from a variation of the specific ionization along the track inside the chamber. Since the  $E'_2(x)$  curve is steeper than the  $E'_1(x)$  curve,  $E'_2$  might thus be measured relatively too high, because when the positive ions are not removed, the ion pairs will give rise to the higher pulses, the larger their distances from the collecting plate. However, the errors involved are quite negligible; for instance, for the measurements near the beginning of the range,  $E'_2$  decreases by about 5 per cent along the track inside the chamber and, if  $E'_1$  were constant along the track, the error would amount to less than 0.8 per cent.

Another possible source of error is that an ion multiplication occurs in the chamber. Such a multiplication would probably also favorize  $E'_2$ , because the chance that an electron produces a new ion pair must be assumed to be proportional to the distance traversed by the electron and because the  $E'_2$  curve is the steeper one. However, if such a multiplication were present, and if it distorted the results, one should expect the ratio between pulses corresponding to the two groups to vary strongly with the voltage across the chamber, which is not the case. This is proved by Fig. 5 for a pressure of 300 mm Hg. Similar investigations

giving the same result were also performed at lower pressures, 150 and 75 mm Hg.

At first sight, it might seem surprising that the range-ionization curves for the two groups intersect; nevertheless, this is just what should be expected. The heavy group is known to have the lower initial velocity and, since it has the higher initial charge (7), it must also be expected to have the higher initial ionization in agreement with the result of the present experiments. Then, because the heavy group has the shorter range, the curves must intersect.

## CHAPTER II

### Specific Ionization in Various Gases.

#### § 1. Specific ionization in xenon.

Using the apparatus described in Chapter I the specific ionization was measured in several gases.

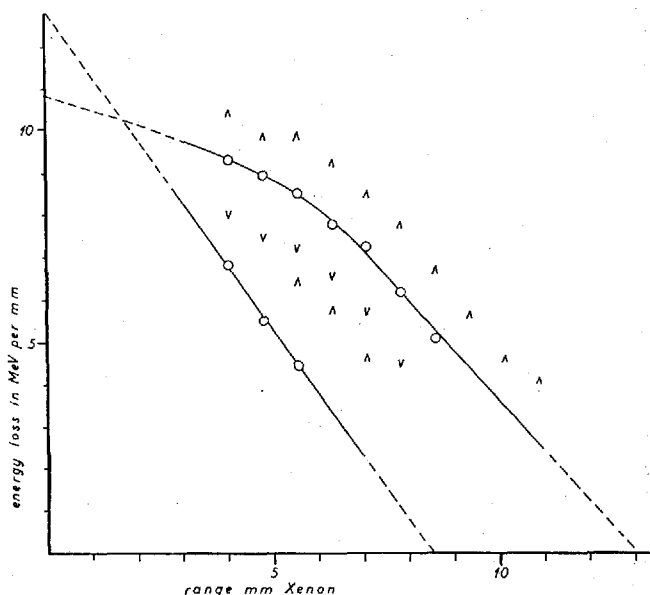


Fig. 14. Ionization range curves in xenon. Open circles correspond to peak values, arrow points to upper and lower limits.

In xenon two series of measurements were performed at a pressure of 115 mm Hg and 38 mm Hg. Since some of the recording films were lost by an accident the transformation factor necessary for a comparison of the two series of measurements could not be determined, but the experimental results were found to be very similar to those in argon, the higher stopping power of xenon of course being taken into consideration. For  $x$ -values of 1.9 and 2.9 mm xenon the distribution curves were very similar to those for  $x$ -values 3.8 and 5.8 mm of argon (Fig. 9), showing a single, rather symmetrical peak and a peak with a hump on the left side, respectively.

Fig. 14 gives the result of the measurements at a pressure of 115 mm Hg. The extrapolated ranges  $R_{ex}$  are found to be 8.5 and 13 mm of xenon, corresponding to 16 and 24 mm of air<sup>1</sup>, which is slightly higher than the corresponding values obtained in argon (13.5 and 21.7 mm of air), but the differences are hardly outside the limits of experimental error. The ratio of the areas beneath the two curves is  $86:54 = 1.60$ , in rather good agreement with the value given by FLAMMERSFELD et al.

#### § 2. Specific ionization in the light gases.

Preliminary experiments with the first diaphragm and the aluminum foil showed that the ionization distribution curves found in hydrogen, deuterium, and helium were similar to those in argon, the ionization varying along the range in much the same way. However, rather large differences concerning the reduced extrapolated ranges occurred<sup>1</sup>. Also, the magnitude of the background relative to the actual pulses varied from one gas to another; in hydrogen it was slightly higher than in deuterium, and in helium it was considerably higher.

All three gases were used at a pressure of 120 mm Hg (15° C).

<sup>1</sup>) The reduced extrapolated range is here defined by the expression

$$R_{ex}^{air} = R_{ex} \cdot \sigma \cdot \frac{n}{2},$$

being the relative stopping power for  $P\sigma\alpha$ -particles and  $n$  the number of atoms in the molecule.

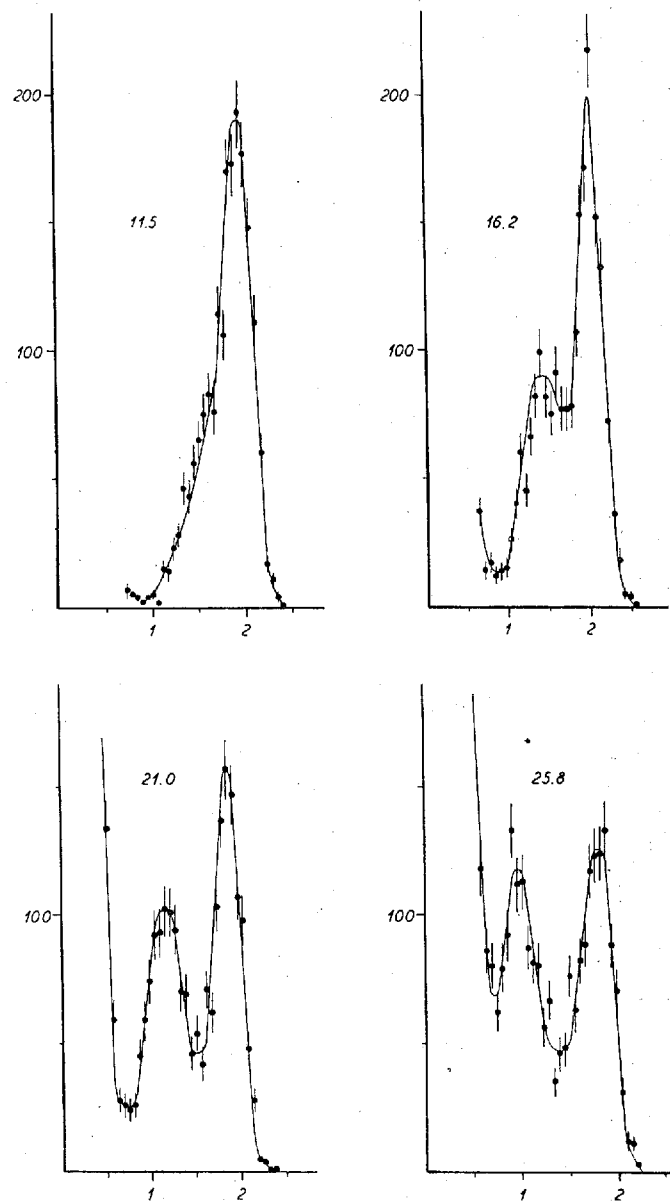


Fig. 15. Ionization distribution curves in deuterium corresponding to distances between uranium layer and ionization chamber ranging from 11.5 to 25.8 mm.  $D_2$ .—Ordinate: number of fragments.—Abscissa: size of pulses in MeV per mm  $D_2$ . (For the calibration of the pulse sizes, see text.)

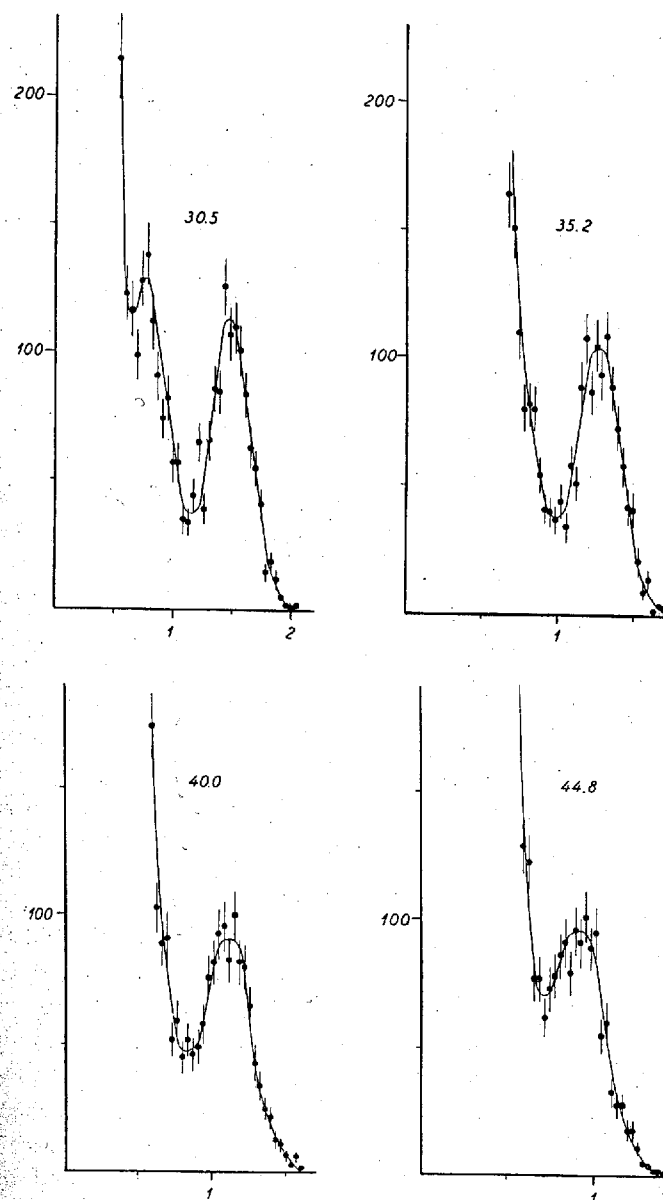


Fig. 16. Specific ionization in deuterium for  $x$  values ranging from 30.5 to 44.8 mm.

From the reduced ranges given by BØGGILD, ARRØE, and SIGURGEIRSSON (10<sup>4</sup>) for the light fragment, 21.1, 22.5, and 28 mm of hydrogen, deuterium, and helium, respectively, it was estimated that a suitable range interval would be covered by the arrangement. However, it turned out that the reduced extrapolated ranges  $R_{\text{ex}}^{\text{air}}$  were much smaller, viz. 14.1, 15.1, and 19 mm of air in H<sub>2</sub>, D<sub>2</sub>, and He, respectively. Consequently, a rather large fraction of the total ionization curve had elapsed for  $x$  values smaller than those covered by the measurements and only a few points in the end of the curve for the light group were obtained.

In order to investigate a larger part of the range and to obtain information about the heavy group, it was decided to repeat the experiments with the second diaphragm and a gold foil. As in the preliminary experiments the hydrogen was taken from a steel tank, but before entering the chamber it was passed slowly over red-hot copper and through a liquid air trap. The deuterium was produced by electrolysis from heavy water containing about 5 per cent NaOH and was purified in the same way. The helium was taken from a steel tank; as it was assumed to be pure, only containing traces of nitrogen, it was not purified any further. Later, the helium was weighed; when the gas is assumed to be a mixture of He and N<sub>2</sub>, an assumption which is justified in view of a spectroscopical analysis earlier performed by Professor E. Rasmussen, the amount of N<sub>2</sub> was found to be 2.8 per cent.

The same pressure, about 720 mm Hg, was used with all three gases and, since all measurements for the various  $x$ -values were performed at this pressure, no transformation factors were required. The thickness of the gold foil, 0.18 mg/cm<sup>2</sup>, was put equal to 2.0 mm of H<sub>2</sub> or D<sub>2</sub> and to 2.3 mm of He.

The results of the experiments agree with the preliminary results. Figs. 15 and 16 show some of the distribution curves obtained in D<sub>2</sub>. The curves obtained in H<sub>2</sub> were almost identical with the former. In He, very similar curves were obtained, but due to the higher background the peaks were slightly broader and the separation between the peaks and the background was somewhat less complete (cf. Fig. 17).

<sup>1</sup>) In the following cited as B. A. S.

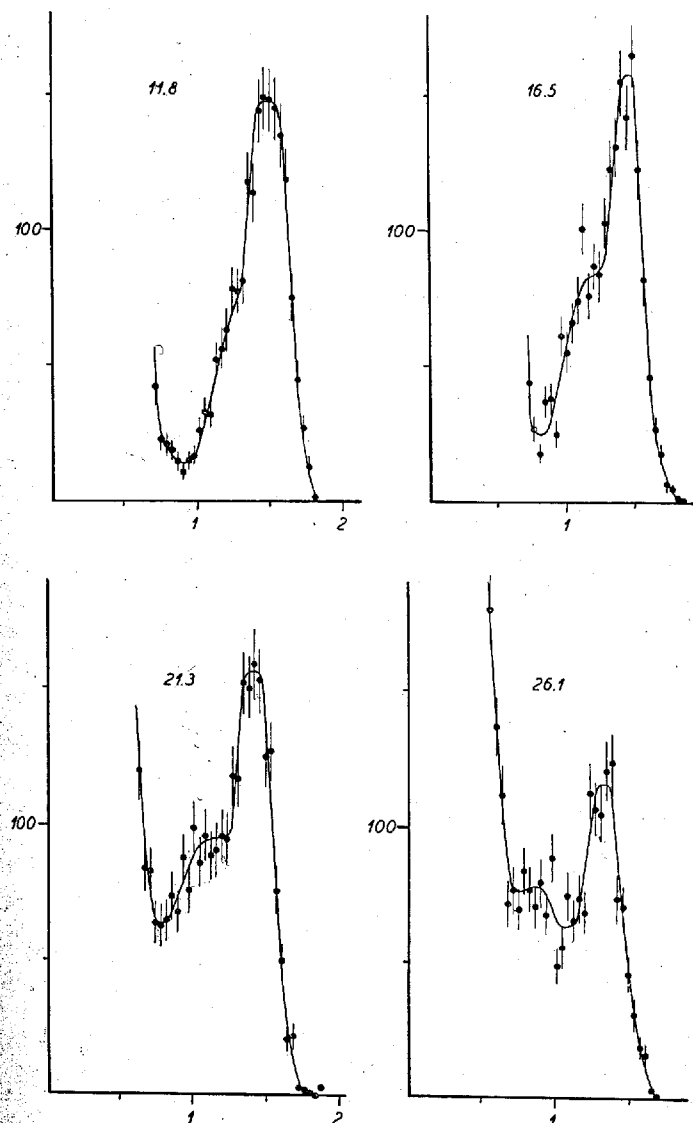


Fig. 17. Specific ionization in helium for  $\alpha$  values ranging from 11.8 to 26.1 mm.

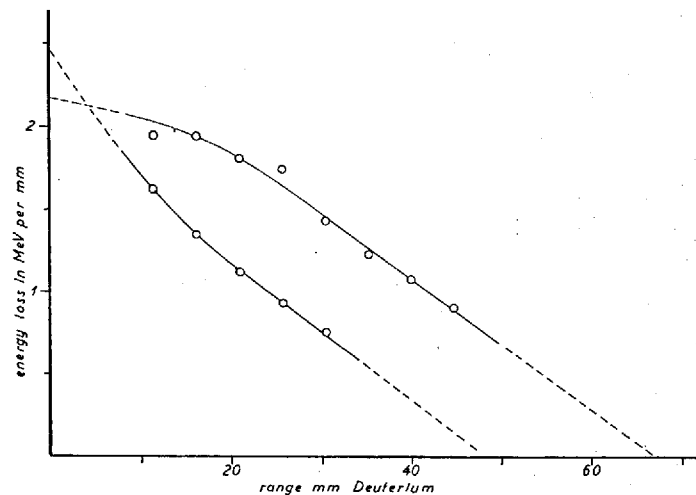


Fig. 18. Ionization range relations in deuterium.

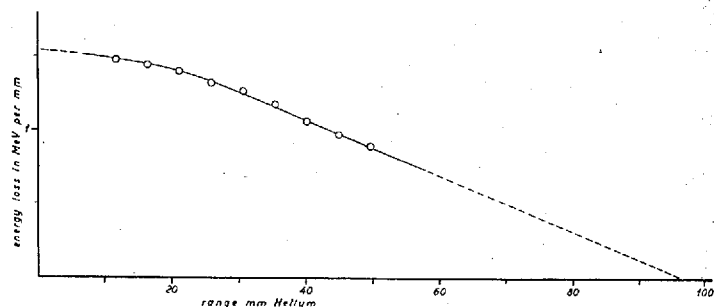


Fig. 19. Ionization range relation for the light fragment in helium.

Fig. 18 gives the ionization range curves in  $D_2$ , which are nearly identical with those in  $H_2$  (cf. Chapter III). The ratio between the areas beneath the two curves is found to be  $86.52 = 1.65$ , which is the same as in A.

Fig. 19 gives the range ionization curve for the light group in He. Unfortunately, no reliable curve for the heavy fragment can be derived from the measurements, but in Fig. 17 it is indicated that the point of intersection of the two curves, if any, falls close to the starting point of the fragments.

### § 3. Comparison of various gases.

The ionization range curves in the light gases show some differences from the corresponding curves in argon.

(1) The curve for the heavy group in A is nearly a straight line; in  $H_2$  and  $D_2$  the four last points corresponding to  $x$ -values from 16.5 to 30.5 mm fall almost on a straight line, but the point for  $x = 11.5$  mm falls somewhat above the line both in  $H_2$  and in  $D_2$ . This point is the most uncertain one, because the corresponding ionization distribution curve shows only one peak which is the sum of the two peaks corresponding to the two groups. However, as these two peaks cover equal areas, it is possible to analyse the curve and to determine the approximate position of the two peaks. Thus, the curve in  $H_2$  and  $D_2$  is found to be somewhat bent; in fact, the last four points also indicate a small curvature of the line.

(2) In  $H_2$  and  $D_2$  as well as in A the curves corresponding to the light fragment are straight lines for the intermediate part of the range, which has been used to define the extrapolated ranges, and in all three gases  $E_1$  decreases more slowly in the beginning of the path. However, the bend of the curve in A occurs at an  $x$ -value about half the extrapolated range, while in  $H_2$  and  $D_2$  it falls somewhat nearer the beginning of the path.

(3) The curves corresponding to the two groups of fragments will possibly intersect in all three gases, but in  $H_2$  and  $D_2$  the point of intersection is situated much nearer the origin than it is in A; in fact, from the experimental results we cannot at all deduce with certainty that the curves will intersect in the light gases. In  $H_2$  an ionization distribution curve was determined for an  $x$ -value of 4.5 mm; this curve had only one rather symmetrical peak, which justifies the way in which the curves are extrapolated towards small  $x$ -values.

(4) The ranges obtained in the various gases are summarized in Table 4.  $\sigma$  denotes the value of the relative atomic stopping power used when calculating the reduced extrapolated ranges

from the expression  $R_{\text{ex}}^{\text{air}} = R_{\text{ex}} \cdot \sigma \cdot \frac{n}{2}$ , where  $n$  is the number of atoms in the molecules of the gas. In order to compare with the

Table 4.

	$\sigma$	Extrapolated ranges (present work)				Ranges given by B. A. S.			
		mm of gas		mm of normal air		$\frac{R_{ex^2}}{R_{ex^1}}$	mm of normal air		$\frac{R_2}{R_1}$
		$R_{ex^1}$	$R_{ex^2}$	$R_{ex^1}^{air}$	$R_{ex^2}^{air}$		$R_1^{air}$	$R_2^{air}$	
H <sub>2</sub>	0.22	65.5	47.5	14.4 (14.1) <sup>2</sup>	10.5	0.72	21.1	17.7	0.84
D <sub>2</sub>	0.22	68	48.5	15.0 (15.1) <sup>2</sup>	10.7	0.71	22.5	18.9	0.84
He <sup>1</sup>	0.395 <sup>1</sup>	97		19 (19) <sup>2</sup>			28	23	0.82
A	1.94	22.4	14.4	21.7	14.0	0.65	23.9	19.4	0.81
Xe	3.76	13	8.5	24	16	0.67	23	18	0.81

<sup>1</sup> As the helium gas was a mixture of 97.2% He and 2.8% N<sub>2</sub>,  $\sigma$  was put equal to  $0.35 \cdot 0.972 + 2 \cdot 0.98 \cdot 0.028 = 0.395$ ; 0.35 and 0.98 being the stopping powers for He and N<sub>2</sub>, respectively.

<sup>2</sup> The figures in the brackets are those obtained in the preliminary investigations.

total reduced ranges given by B. A. S. the stopping power for Po  $\alpha$ -particles is chosen.

It is seen that the air equivalent of the extrapolated ranges increases monotonically with the atomic number of the stopping

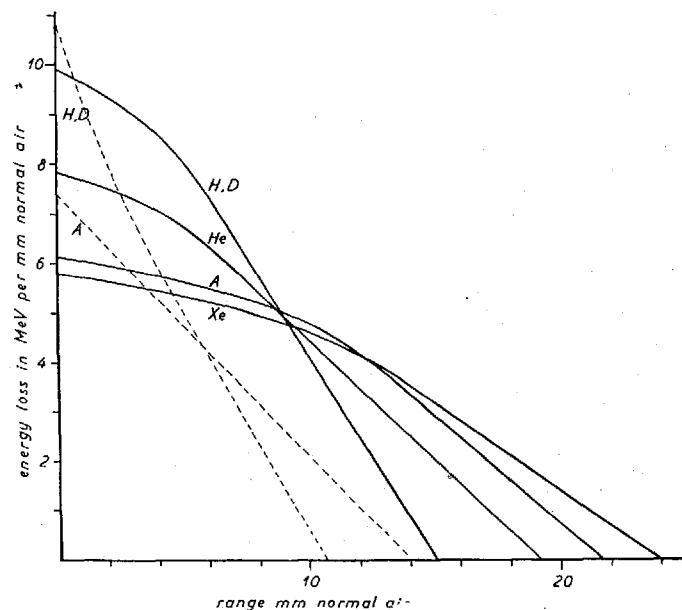


Fig. 20. Ionization range relations in various gases.—The full-drawn curves correspond to the light group, the dotted lines to the heavy group.

gas, in contrast to the total reduced ranges given by B. A. S., which decrease from He through A to Xe. This is by no means a discrepancy, as will be further discussed in Chapter III.

In Fig. 20 are plotted the ionization range curves for the various gases; the abscissae are the distances traversed, reduced to normal air by means of the values for  $\sigma$  given above. Evidently, the small values of the reduced extrapolated ranges in H<sub>2</sub>, D<sub>2</sub>, and He involve a higher initial ionization per mm of air in these gases than in A, a result which, however, is in agreement with the theory. Moreover, the agreement is not only qualitative. From the figure we find for the ionization per mm of air, i. e. the ionization by fission fragments relative to that by  $\alpha$ -particles, that for the light group it is 1.6 times higher in H<sub>2</sub> (D<sub>2</sub>) than in A, and 1.2 times higher in He than in A. Assuming the charge to be the same in all gases, BOHR (2) finds the ratios, calculated by means of the theoretical stopping formula, to be 1.5 and 1.2, respectively, in agreement with the experimental values.

#### § 4. Measurements in mixtures of gases.

Although the above-mentioned agreement is rather satisfactory, the ionization in H<sub>2</sub> is seen to be slightly higher than

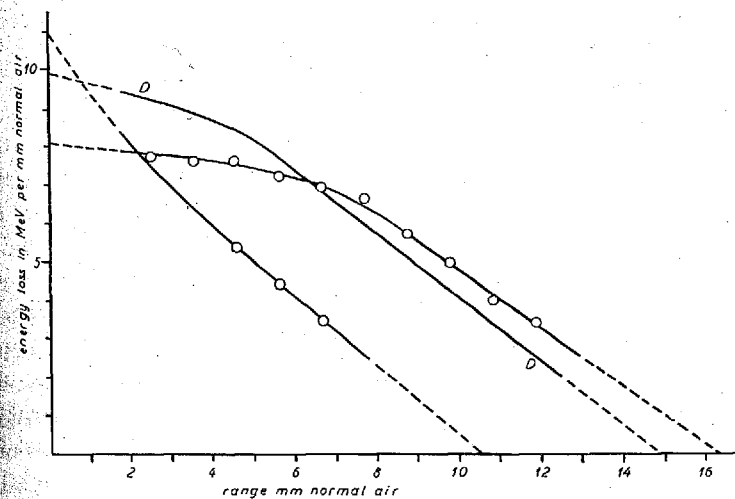


Fig. 21. Ionization range relations in a mixture of 95 per cent deuterium and 5 per cent argon.—The curve D-D corresponds to the light group of fragments in pure D<sub>2</sub>. The curves for the heavy group in pure D<sub>2</sub> and in the mixture, respectively, are identical.

what corresponds to the calculations. This might indicate that also the charge in  $H_2$  is slightly higher than in the other gases, which would not be difficult to understand from a theoretical point of view. For  $\alpha$ -particles the cross-section for electron capture is much smaller in  $H_2$  than in heavier gases and the same should be true for fission fragments. One should thus expect that a small admixture of a heavier gas would cause an increase in the charge and the ionization; measurements of the specific ionization were therefore performed in two gas mixtures.

In a mixture of 564 mm  $D_2$  and 30 mm A the result shown in Fig. 21 was obtained.  $R_{ex-1}^{air}$  is found to be somewhat higher than in pure  $D_2$  (16.4 mm of air against 15.0), but  $R_{ex-2}^{air}$  is unchanged. For a comparison the curves obtained in pure  $D_2$  are shown. The curves for the heavy group are identical, while those for the light group differ markedly. For  $x = 2.3$  and 3.2 mm no points are given for the heavy group, since only one peak is seen on each of the corresponding distribution curves and their analysis is rather uncertain, but from the distributions it is obvious that the curves intersect at an  $x$ -value near 2. Thus, it is found that the point of intersection has a higher  $x$ -value and that the bend of the curve for the light group falls at higher  $x$ -values than in pure  $D_2$ . The features of the curves approach those in A, but the change is by far the highest for the light fragment. For this fragment the initial specific ionization is much lower in the mixture than in pure  $D_2$ , but even if the charges in the two gases are equal, the ionization will of course be the smaller in the mixture. However, a closer examination of the results indicates a lower  $z_1^*$  value in the mixture (see Chapter III).

The determination of the ionization range curves in the mixture of  $D_2 + A$  is based on measurements of about 17,000 pulses, a number of the same order of magnitude as that used when determining the curves in the pure gases. In a mixture of 560 mm  $He + 28$  mm A similar measurements were performed, but only  $1/4$  of the recording films were examined, as the distribution curves were found to be almost identical with those in helium without the admixture of A.  $R_{ex-1}^{air}$  was found to be the same in the mixture containing A and in helium, only containing the admixture of  $N_2$  (19.5 and 19.2 mm of air, respectively).

### CHAPTER III

## Construction of Velocity Range Relations for the whole Range.

### § 1. Energy loss along the range in argon.

The previous measurements of the specific ionization could only yield ionization range curves for the first part of the range since, in the last part of the range, the ionization became too low as compared with the ionization background in the chamber. However, even if the ionization had been measurable, we could not, as in the beginning of the path, expect it to be proportional to the energy loss, since in the end of the path ionization takes place mainly through nuclear collisions and since many of the recoiling atoms might have rather small energies and, hence, produce fewer ion pairs per eV. If for velocities of the fragments smaller than  $v_0 = \frac{\epsilon^2}{\hbar}$  the energy loss due to electronic encounters is neglected in comparison with that due to nuclear collisions, the energy loss may be estimated by the formula (BOHR, ref. 2, formula 5.1.2)

$$-\frac{dv}{dx} = 2\pi N \frac{z^2 z'^2 \epsilon^4}{mm'v^3} \cdot L_v, \quad (1)$$

where  $L_v$  is a logarithmic expression which may be written

$$L_v = \log \left\{ z z' \sqrt{z^{2/3} + z'^{2/3}} \cdot \frac{\mu (m + m')}{mm'} \cdot \left( \frac{v_0}{v} \right)^2 \right\}. \quad (2)$$

In these expressions,  $N$  denotes the number of atoms per  $cm^3$  of the stopping gas, and  $m$  and  $z$  are the mass and the nuclear charge numbers of the fragment, while  $m'$  and  $z'$  refer to the gas atoms, and  $\mu$  is the electronic mass.

Formula (1) does not hold for very small velocities  $\left( v < \frac{1}{3} v_0 \right)$  for which the logarithmic argument in (2) becomes comparable

with or smaller than unity. For such velocities  $-\frac{dv}{dx}$  will vary inversely proportional to  $v$ , but in the case of fission fragments this problem affects only the extreme end of the range and is insignificant in the present connection.

Let us consider the "average fragments" to which we ascribe the values  $(z_1, m_1) = (39, 95)$  and  $(z_2, m_2) = (53, 139)$  (cf. ref. 11). By a numerical integration of (1) we get  $v$  and  $\frac{dv}{dx}$  as functions of  $x$  in the range interval concerned. Fig. 22 shows the result for the light fragment; the point for which  $v = v_0$  has been chosen as origin on the axis of abscissae. From these two curves  $\frac{dE}{dx} = mv \frac{dv}{dx}$  is calculated and the result is given by curve *a* in Fig. 23. The endpoint for this curve has been chosen to be  $x = 2.47$  cm of argon in accordance with the range value given by B. A. S. Curve *b* of Fig. 23 is the curve from Fig. 13 corresponding to the most frequent values of the specific ionization for the light group, and the full-drawn curve obtained by fitting together *a* and *b* in the way shown in the figure may be assumed to represent

the  $\frac{dE}{dx}$  curve along the whole range for the fragment with  $(z_1, m_1) = (39, 95)$ . In order to derive this curve, the curves *a* and *b* should, strictly speaking, be plotted as functions of the velocity, in which case the contributions from electronic and nuclear collisions could be directly added. However, considering the uncertainty of the whole procedure, it is justified simply to join *a* and *b* in a smooth way.

The corresponding curve for the heavy fragment has been obtained in a similar way and is also shown in Fig. 23. The ordinates of the ionization measurements, determined only on a relative scale, have been normalized in such a manner that the area beneath the full-drawn curve for the light fragment is 86 MeV

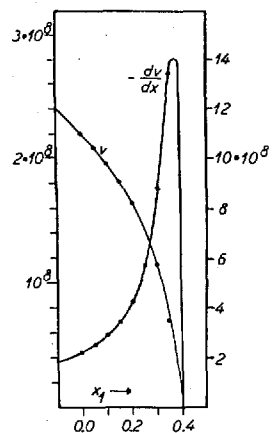


Fig. 22.  $v(x)$  (scale to the left) and  $-\frac{dv}{dx}(x)$  (scale to the right) for the light fragment in argon. The curves are calculated on the assumption that the energy loss is due entirely to nuclear collisions.

representing the initial energy. The area beneath the curve for the heavy fragment is then found to be 55 MeV, corresponding to a ratio 1.56 between the initial energies of the two fragments, in good agreement with the value of 1.50 given by FLAMMERSFELD et al. (6) and the value of 1.49 given by JENTSCHKE (12). It is of interest here to note that the ratio of the areas beneath

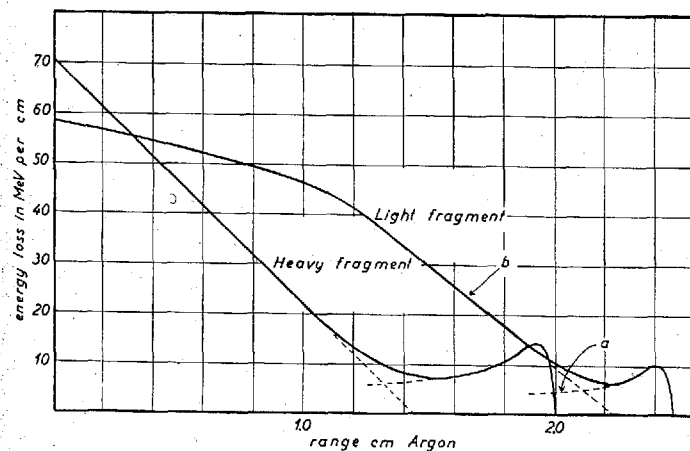


Fig. 23. Energy loss along range in argon.

the two extrapolated ionization curves is 1.65, which is higher than the directly measured ratio of the initial energies and, thus, that we get an improved internal consistency of the empirical data by taking into account the difference between  $R_{ex}$  and  $R$ .

## § 2. Energy range curves and velocity range curves in argon.

From the  $\frac{dE}{dx}$  curves the  $E(x)$  curves are obtained by integration. Fig. 24 shows the result for both fragments. The curve for the light fragment may be compared with the curve previously measured in mica (3). Assuming the relative stopping power of argon and mica to be the same for fission fragments as for  $\alpha$ -particles of medium velocity, for which 1 cm of argon corresponds to 1.41 mg/cm<sup>2</sup> of mica, we get a very close agreement, the difference between the two curves in the interval from 0 to

2.4 mg/cm<sup>2</sup> of mica never exceeding 2 MeV. For fragments having traversed 1.04 mg/cm<sup>2</sup> of mica, corresponding to 0.74 cm argon,  $E_2$  was previously found to be 23 MeV (13), while the corresponding value as taken from Fig. 24 is 19 MeV. Also here it is interesting to note that, if the tail of the  $\frac{dE_2}{dx}$  curve had been omitted, we would have obtained an  $E_2(x)$  curve giving the value

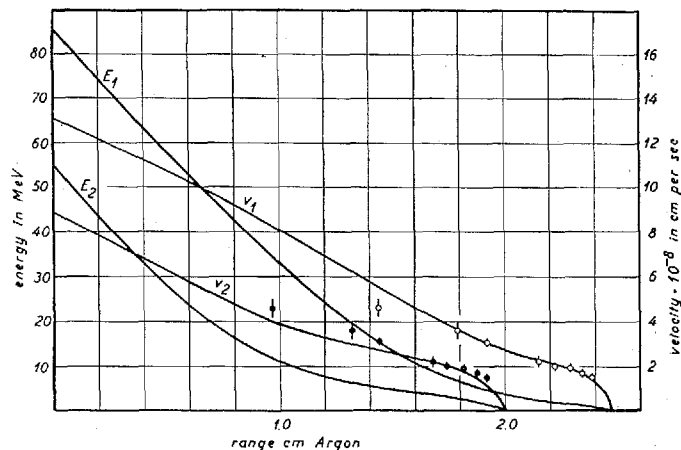


Fig. 24. Energy vs. range (scale to the left) and velocity vs. range (scale to the right) for fission fragment in argon. Indices 1 and 2 refer to the light and heavy group, respectively. The points are the velocities given by Bøggild, Brøstrøm, and Lauritsen.

of 12 MeV, which would be in definite disagreement with the measured 23 MeV.

From the  $E(x)$  curves also the  $v(x)$  curves may be derived. They are shown in the same figure where furthermore are plotted the results obtained by BØGGILD, BRØSTRØM, and LAURITSEN (1) who have measured the velocity as a function of the residual range. These authors give mean values for both groups of fragments taken together and, consequently, their data have been compared with the curve for the light fragment (open circles) as well as with the  $v_2(x)$  curve (full circles). The points are seen to fall slightly below the  $v_1(x)$  curve and slightly above the second curve; thus the agreement must be considered satisfactory.

### § 3. Energy loss along the range in the light gases.

In complete analogy to the procedure described in § 1 the  $\frac{dE}{dx}$  relations have been constructed for H<sub>2</sub> and D<sub>2</sub> by means of the measurements of specific ionization, the nuclear stopping

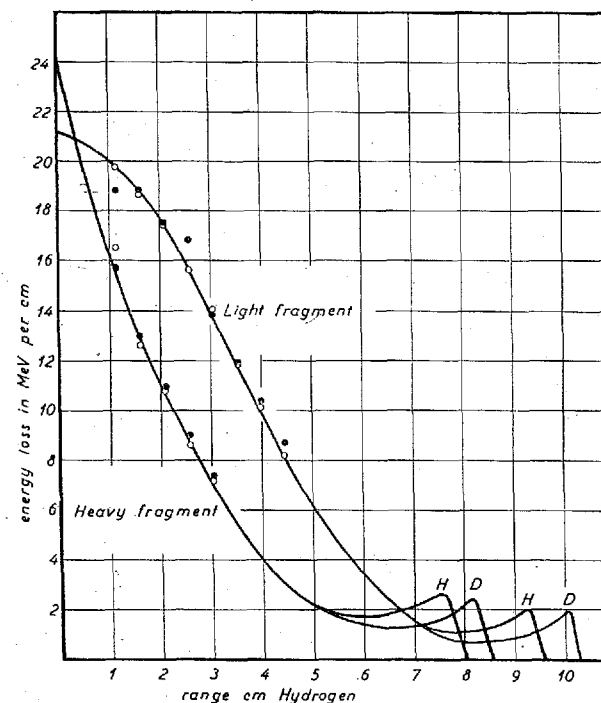


Fig. 25. Energy loss along range in hydrogen and deuterium. The open circles are the experimental values found in H<sub>2</sub>, the full circles the corresponding values in D<sub>2</sub>.

formula (1), and the range values given by B. A. S. The result is shown in Fig. 25. It should here be remembered that the experimental values are measured only in relative units and, hence, the agreement between the absolute values of the points corresponding to H<sub>2</sub> and D<sub>2</sub> is partly a result of the normalization of the scale, by which the areas beneath the curves for the light fragment in H<sub>2</sub> and D<sub>2</sub> are given the same value. Nevertheless, it is satisfactory to find that the rate of decrease in specific energy loss for the light fragment in the first part of the path is so nearly

the same in the two gases and that also the two curves for the heavy group coincide. This not only checks the reliability of the measurements, but it also confirms the theoretical estimate that the stopping in this part of the range is due to electronic encounters and that nuclear collisions are of negligibly small influence.

The influence of nuclear collisions over the last part of the range is exhibited by the difference of the ranges in  $H_2$  and  $D_2$ . This difference can be estimated on the assumption that, as a first approximation, electronic stopping may be neglected for velocities smaller than  $v_0$  and that nuclear stopping is unimportant for  $v > v_0$  (2). In this way, one finds differences of 7 mm and 5 mm for the light and heavy fragment, respectively, which is just in accordance with the empirical values found by B. A. S.

The ratio of the areas beneath the  $\frac{dE_1}{dx}$  curve and the  $\frac{dE_2}{dx}$  curve is found to be 1.53, in agreement with the measured ratio of the initial energies.

#### § 4. Energy range curves and velocity range curves in $H_2$ and $D_2$ .

In a manner similar to that applied for argon the  $E(x)$  curves and the  $v(x)$  curves are derived for  $H_2$  and  $D_2$ . They are shown in Fig. 26, where also the  $v(x)$  values obtained in  $H_2$  (open circles) and  $D_2$  (full circles) by B. A. S. are plotted. It is seen that these values fall rather far outside the curves; the discrepancy cannot be explained only by uncertainties in measurements, but seems to represent a systematic deviation. In fact, the points are situated nearly on the straight lines connecting the two ends of the curves (dotted on the figure) and from the preceding procedure it is clear that when representing  $v(x)$  by these lines we would find disagreement with the theory as well as with the measurements of the specific ionization.

A possible explanation for the discrepancy might be found in the assumption that the light gases in the cloud-chamber used by B. A. S. were not pure, but contained admixtures of heavier

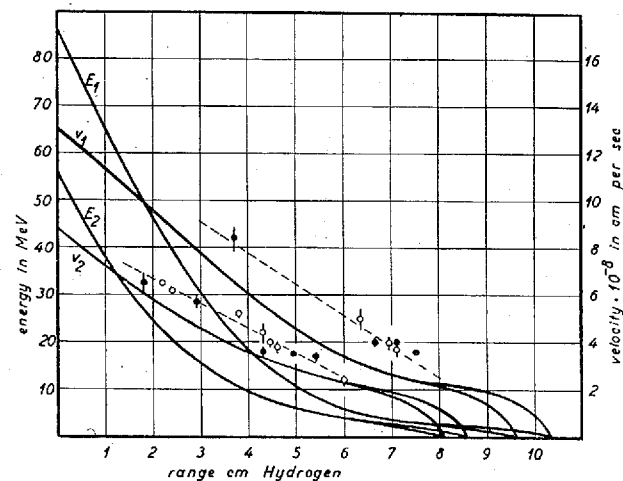


Fig. 26. Energy vs. range (scale to the left) and velocity vs. range (scale to the right) for fission fragments in hydrogen and deuterium.—Indices 1 and 2 refer to the light and heavy fragment, respectively.—The points are the velocities given by Bøggild, Arrøe, and Sigurgeirsson, the open and full circles corresponding to  $H_2$  and  $D_2$ , respectively.

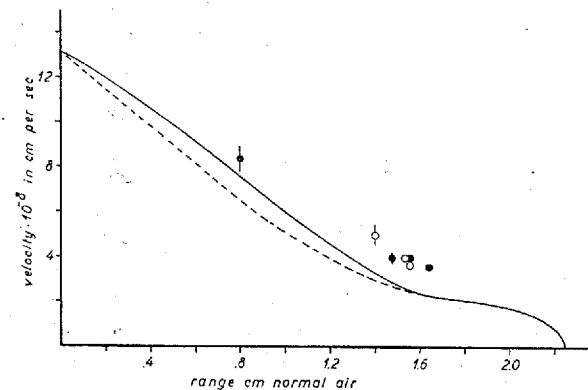


Fig. 27.

gases; in any case, we know that some water vapour was present. As will be seen from Fig. 21, a small contamination of argon in the deuterium gas causes a rather large change of the  $\frac{dE_1}{dx}$  curve. The effect is much smaller for the heavy fragment, but in this connection it might also be noted that the deviation of the cloud-chamber data from the curves in Fig. 26 is much

greater for the light than for the heavy fragment. In order to estimate the influence of impurities we may use the ionization measurements in a mixture of 95 per cent D<sub>2</sub> and 5 per cent A, given in Fig. 21. From these measurements the velocity range relation can be calculated in the usual way by assuming the total range to be equal to those given by B. A. S. for their deuterium gas. The  $v_2(x)$  curve is not appreciably different from that in Fig. 26;  $v_1(x)$  for the mixture is shown by the full-drawn curve in Fig. 27, while for pure D<sub>2</sub>  $v_1(x)$  is represented by the dotted curve. It is seen that the new curve comes somewhat nearer to the cloud-chamber data in the first part of the range, but it is at the same time evident that in this manner no explanation is offered of the discrepancies at smaller velocities.

However, there is no reason to emphasize this discrepancy. The cloud-chamber data cannot be expected to have a high accuracy in the velocity region concerned, since they rely on the proton velocity range relation which is not very well known for such small velocities. Moreover, the greatest uncertainty of the constructed velocity range curves falls just in the region in question, in which nuclear stopping gradually takes over from electronic stopping. In fact, the curves have been constructed in accordance with the assumption that electronic stopping may be neglected for  $v < v_0$ ; this assumption, of course, is somewhat arbitrary, although it was seen to give the correct values for the differences of the ranges in H<sub>2</sub> and D<sub>2</sub>.

### § 5. Estimate of the effective charge of the fragments.

From the values of  $\frac{dE}{dx}$  along the range it is possible to calculate the effective charge  $z^*$  of the fragments by means of the electronic stopping formula (BOHR, ref. 2, formula 5.1.2)

$$-\frac{dE}{dx} = 2\pi N \frac{(z^*)^2 \epsilon^4}{\mu v^2} \cdot L_e. \quad (3)$$

In heavy stopping materials like A the quantity  $L_e$  for fission fragments may be obtained from the relation

$$L_e = L_e^\alpha \left( \frac{3}{4} x^{-\frac{1}{3}} + \frac{1}{4} x^{-1} \right), \quad (4)$$

where

$$x = 2 z^* \cdot \frac{v_0}{v} \quad (5)$$

and where  $L_e^\alpha$  is a quantity to be used in (3) when  $\alpha$ -particles are considered. This quantity may be derived from the measurements of MANO (14) of the stopping of  $\alpha$ -particles in A. He finds that the empirical data can be represented by the expression

$$L_e^\alpha = z \log \left( \frac{2\mu v^3}{\bar{I}} \right)^2 \quad (6)$$

with  $\bar{I} = 195 \text{ eV}^1$ . MANO's measurements cover only velocities greater than  $12 \cdot 10^8 \text{ cm/sec}$ ; for considerably smaller values (6) will not hold but, since  $L_e^\alpha$  according to (6) is nearly linear for a large interval of  $v$  and since, according to general arguments (2),  $L_e^\alpha$  should be approximately proportional to  $v$  over a large velocity region, we may extrapolate towards smaller  $v$  by the expression

$$L_e^\alpha = 6.33 \cdot 10^{-8} \cdot v \quad (7)$$

which coincides with (6) for  $v = 13.1 \cdot 10^8 \text{ cm/sec}$ .

The calculated values of  $z^*$  for the two fragments are shown in Fig. 28 as functions of  $x$  and of  $v$ . The initial effective charges are found to be about  $22 \epsilon$ , which closely coincides with the measured values of the total charges  $e$  of the fragments (5). Through the end-points of the  $z^*(v)$  curves are drawn dotted curves proportional to  $v$  (curves *a* and *b*) and proportional to  $v^{\frac{1}{2}}$  (curve *c*). In earlier experiments (3), the total charge  $e_1$  for the light fragment was found to be nearly proportional to  $v_1^{\frac{1}{2}}$  in the beginning of the range, and the corresponding quantity  $e_2$  for the heavy fragment was by similar measurements found to decrease somewhat more slowly than  $v_2$ . Concerning the present results it is seen that  $z_2^*$  varies approximately proportional to  $v_2$ .

<sup>1</sup> In fact, in deducing the value  $\bar{I} = 195 \text{ eV}$ , MANO applied certain corrections to formula (6); in our case, however, these are already included in relation (4).

and that  $z_1^*(v)$  decreases more slowly than  $z_2^*(v)$ , in accordance with the mentioned measurements of the total charges.

A slight discrepancy which definitely cannot be accounted for by experimental uncertainties appears since, according to Fig. 28, we have  $z_1^* > z_2^*$  for  $x = 0$ , while the charge measure-

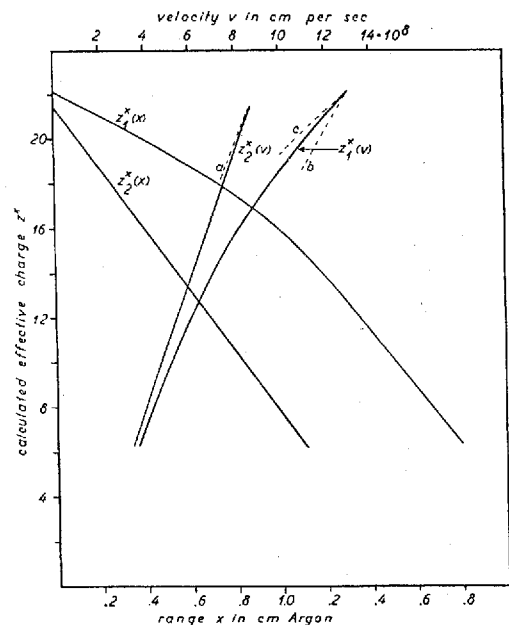


Fig. 28. The effective charge of fission fragments in argon as functions of the distance  $x$  traversed (scale of abscissae below) and as functions of the velocity  $v$  (scale of abscissae above).

ments (9) have shown that the heavier fragment at the beginning of the range carries a charge about 10 per cent higher than that of the lighter fragment. A possible, though not very probable explanation for this discrepancy might be found in the fact that the measured charge values are those characteristic of the penetration of the fragments through the uranium target, while the values in Fig. 28 correspond to argon. Another explanation would be that the effective charge, as defined by (3), although approximately equal to the total charge of the fragment, still might differ slightly from this quantity.

In the case of hydrogen, the value of  $L_E$  to be introduced in (3) may be written

$$L_E = \log \left\{ \left( \frac{2v}{v_0} \right)^4 [\kappa]^{-2} \left[ \kappa \cdot \frac{v_0}{2v} \right] \right\}, \quad (8)$$

where the square brackets indicate that the quantity in the brackets is to be replaced by unity if smaller than 1. A slightly more

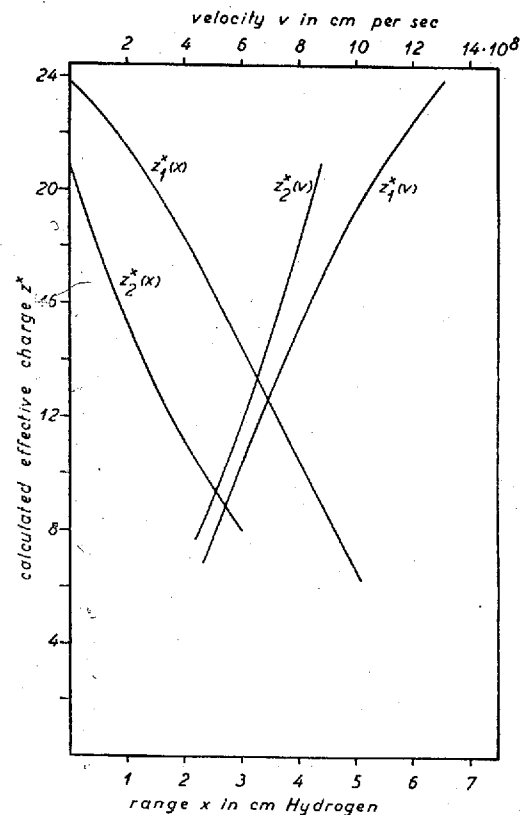


Fig. 29. The effective charge of fission fragments in hydrogen as functions of the distance  $x$  traversed (scale of abscissae below) and as functions of the velocity  $v$  (scale of abscissae above).

accurate expression is obtained by replacing  $v_0$  by  $v_H$  given by  $\mu v_H^2 = 16.0 \text{ eV}$ , since expression (8) in the case of fast  $\alpha$ -particles for which  $\kappa < 1$  reduces to MANO's semi-empirical formula.

The calculated values of  $z^*$  in  $\text{H}_2$  are shown in Fig. 29. The curves are similar to those in argon and also here the initial

value of  $z^*$  is higher for the light than for the heavy fragment. As is seen, the initial values of  $z_2^*$  are approximately equal in the two gases, while  $z_1^*$  is slightly higher in  $H_2$  than in A.

Similar calculations for the mixture of 95 per cent  $D_2$  and 5 per cent A lead to the result that the heavy fragment has almost the same initial effective charge in all the gases, while the initial value of  $z_1^*$  was found to be about 10 per cent lower in the mixture than in pure  $D_2$ .

Thus, it is indicated that the effective charge for the light fragment has a higher value in the light than in heavier gases. In view of the fact that this result is somewhat uncertain it is planned to measure the total charge in the various gases by means of the deflection method\*).

This work has been carried out at the Institute for Theoretical Physics, University of Copenhagen. The author is deeply grateful to the Director of the Institute, Professor NIELS BOHR, for his continued encouragement. I also wish to express my heartfelt thanks to Professor J. C. JACOBSEN for his great interest in the work and, furthermore, I am indebted to AAGE BOHR, mag. sc., for valuable discussions and suggestions.

### References.

- 1) J. K. BØGGILD, K. J. BROSTRØM, and T. LAURITSEN: D. Kgl. Danske Vidensk. Selskab, Mat.-fys. Medd. 18; no. 4, 1940.
- 2) N. BOHR: D. Kgl. Danske Vidensk. Selskab, Mat.-fys. Medd. 18; no. 8, 1948.
- 3) N. O. LASSEN: Phys. Rev. 69; 137, 1946.
- 4) N. O. LASSEN: Phys. Rev. 70; 577, 1946.
- 5) N. O. LASSEN: D. Kgl. Danske Vidensk. Selskab, Mat.-fys. Medd. 23; no. 2, 1945.
- 6) A. FLAMMERSFELD, P. GENTNER, and W. JENSEN: ZS. f. Phys. 120; 450, 1943.
- 7) P. DEMERS: Phys. Rev. 70; 974, 1946.
- 8) R. SHERR and R. PETERSON: Rev. Sc. Instr. 18; 567, 1947.
- 9) N. O. LASSEN: Phys. Rev. 68; 142, 1945.
- 10) J. K. BØGGILD, H. ARRØE, and T. SIGURGEIRSSON: Phys. Rev. 71; 281, 1947.
- 11) The Plutonium Project: Rev. Mod. Phys. 18; 513, 1946.
- 12) W. JENTSCHKE: ZS. f. Phys. 120; 165, 1943.
- 13) N. O. LASSEN: Phys. Rev. 68; 230, 1945.
- 14) G. MANO: Ann. de Phys. (11), 1, 407, 1934.

\*) Note added in proof: As the first results of measurements of the total charge in various gases, the following may be mentioned.

1) In the gases, the light fragment has a higher charge than the heavy fragment, in contrast to the charges as measured in uranium. This result eliminates the discrepancy mentioned on page 40.

2) However, the initial charges are found to be about 15  $\epsilon$ , thus somewhat smaller than the effective charges estimated from the specific energy.

3) The charge of the light fragment may be slightly higher in hydrogen than in heavier gases, but the phenomena seem to be more complicated than assumed in the above paragraph.

More detailed information will be given when the experiments are concluded.